EEET ECOLOGICAL ENGINEERING & ENVIRONMENTAL TECHNOLOGY

Ecological Engineering & Environmental Technology, 2026, 27(5), 359–375
https://doi.org/10.12912/27197050/220571
ISSN 2719–7050, License CC-BY 4.0

Received: 2026.03.19
Accepted: 2026.04.17
Published: 2026.05.01

Port-induced shoreline change and ecological implications in an arid coastal system: Evidence from N'Diago Port, Mauritania

Sidi Ahmed Elemin[1*], Mohammed Fekhaoui[2], Mohamed Ahmed Sidi Cheikh[3], Cristian Pizzigalli[4], Zeinebou Sidoumou[1], Mohamed Avoulwatt[1]

[1] EBIOME Research Unit, Department of Biology, Faculty of Science and Technology, University of Nouakchott, Nouakchott, Mauritania
[2] Laboratory of Ecotoxicology, Scientific Institute, Mohamed V Agdal University, Avenue Ibn Batouta, Rabat, Morocco
[3] GIS and Environmental Expert, Nouakchott, Mauritania
[4] Biopolis Program in Genomics, Department of Biology, Universidade do Porto, Porto, Portugal.
* Corresponding author's e-mail: eddinah98@gmail.com

ABSTRACT

The construction of coastal infrastructure in sediment-limited arid environments can trigger substantial and spatially asymmetric shoreline responses with cascading ecological consequences. This study investigates the morphodynamic and ecological impacts of the Port of N'Diago in Mauritania between 2000 and 2025 by integrating high-resolution satellite imagery and Digital Shoreline Analysis System (DSAS) metrics. A total of 210 transects were established along a 20 km coastal segment – 10 km north and 10 km south of the port – to quantify shoreline changes through net shoreline movement (NSM), shoreline change envelope (SCE), end point rate (EPR), and linear regression rate (LRR). The analysis revealed a pronounced north–south asymmetry in shoreline dynamics: severe erosion occurred south of the port (maximum LRR −18.12 $m \cdot yr^{-1}$), while significant accretion was observed to the north (maximum LRR +8.82 $m \cdot yr^{-1}$), indicating a disruption of natural longshore sediment transport and the establishment of a polarized morphodynamic regime that challenges conventional equilibrium-based coastal models in arid systems. Ecological consequences were assessed by analyzing 80 marine turtle strandings spanning five species, including loggerhead (*Caretta caretta*), green (*Chelonia mydas*), hawksbill (*Eretmochelys imbricata*), leatherback (*Dermochelys coriacea*), and olive ridley (*Lepidochelys olivacea*). Strandings were significantly more frequent near the port, with green turtles accounting for 40% of records. One-way ANOVA revealed a significant effect of port proximity on stranding frequency ($F(1.78) = 7.290$, $p = 0.008$; $\eta^2 \approx 0.085$), confirmed by Welch's robust test ($F(1,24.25) = 5.948$, $p = 0.022$), and a Generalized Linear Model using a Poisson distribution further validated this positive association ($p < 0.05$), providing convergent evidence across parametric, robust, and distribution-adapted analyses. These results demonstrate a direct, quantitative link between engineered shoreline modifications and localized biological impacts, highlighting both the spatial magnitude of port-induced sediment redistribution and its ecological consequences. Limitations include the focus on a single port and arid coastal context, but the methodology offers transferable tools for assessing infrastructure-driven coastal change. The study provides original empirical evidence of how port development can reshape coastal morphodynamics and affect marine biodiversity, offering critical insights for coastal planning, habitat management, and conservation strategies in arid shoreline systems.

Keywords: coastal morphodynamics, DSAS, shoreline change, port infrastructure, sediment transport, marine turtle strandings, Mauritania.

INTRODUCTION

Coastal zones are dynamic interfaces where natural processes and human activities interact, often resulting in pronounced morphological changes (Davidson-Arnott et al., 2019). In arid regions such as Mauritania, these interactions are particularly critical due to ecosystem fragility and limited sediment supply, which constrain the natural capacity of coastlines to recover from disturbance (Lin et al., 2019). The Mauritanian coastline, characterized by low relief and environmentally

sensitive habitats, is increasingly exposed to pressures related to climate change, sea-level rise, and infrastructure development. Among anthropogenic drivers, port construction represents one of the most influential factors affecting coastal dynamics, as it alters longshore sediment transport and disrupts sedimentary equilibrium (Dean and Dalrymple, 2001; Mazières et al., 2014).

The multifunctional port of N'Diago, operational since 2016, provides a relevant case study of these processes. Located near ecologically important areas such as the Diawling National Park, the port supports regional trade, fisheries, and energy logistics, while simultaneously modifying coastal hydrodynamics and sediment pathways. Previous studies have highlighted the vulnerability of the Mauritanian coastline to erosion, a phenomenon often intensified by human intervention (Elmoustapha et al., 2007). However, despite the rapid expansion of port infrastructure along West African coasts, systematic assessments of port-induced shoreline change remain limited, particularly for newly developed infrastructures such as the port of N'Diago.

This study addresses this gap by analysing the spatial and temporal evolution of erosion and accretion patterns along the coastline surrounding the port of N'Diago. Three specific research questions guide the analysis:

1. How has the shoreline evolved before and after the construction of the port?
2. What are the dominant morphodynamic processes (erosion versus accretion), and how are they spatially distributed?
3. How do anthropogenic interventions modify sediment transport pathways and coastal equilibrium?

By addressing these questions, this research aims to provide empirical evidence to support sustainable coastal management in rapidly developing arid regions.

The significance of this study is twofold. First, it advances methodological approaches by integrating multi-sensor satellite imagery (Landsat 7 ETM+ and Landsat 8 OLI, and Sentinel-2A MSI) with the Digital Shoreline Analysis System (DSAS) to quantify shoreline change with high spatial and temporal consistency (Thieler et al., 2009). Second, it delivers policy-relevant insights by highlighting trade-offs between economic development and environmental conservation. Port structures such as jetties may trap sediments locally, promoting accretion in updrift sectors while inducing sediment starvation and erosion in downdrift areas (Mazières et al., 2014). Such effects are particularly critical in arid coastal systems, where natural sediment replenishment is slow and ecosystem resilience is limited (Schlacher et al., 2008).

By combining remote sensing techniques and geospatial analysis, this study provides a reproducible framework for assessing infrastructure-induced coastal change. The findings are particularly relevant for Mauritania and other arid regions where economic development must be balanced with long-term environmental stewardship (Ndour et al., 2018).

STUDY AREA

The port of N'Diago is located in the Keur Macène Department at the southwestern extremity of Mauritania, within the administrative region of Trarza. Positioned near the international frontier with Senegal, the study area lies along the Atlantic Ocean and adjacent to the lower reaches of the Senegal River, forming a strategic coastal interface for regional exchange. The port sits approximately 15 km from the Senegalese city of Saint-Louis (Figure 1), enhancing its significance for transboundary trade and logistics.

The natural environment of N'Diago is characterized by a mosaic of coastal dunes, wetland systems, and estuarine habitats, with the nearby Diawling National Park representing a protected area of high ecological value and biodiversity. This landscape diversity supports a range of ecosystem services and underpins locally important economic activities such as artisanal fishing, irrigated agriculture, and livestock rearing. The juxtaposition of marine, fluvial, and terrestrial environments creates a dynamic coastal system that is both ecologically sensitive and socio-economically vital for the surrounding communities.

Situated at the mouth of the Senegal River, approximately 220 km south of Nouakchott, the port of N'Diago occupies a strategic location along the Mauritanian Atlantic coast. This infrastructure, whose construction began in 2016, comprises several major components: a naval base with a military port, a fishing port equipped with seven berths, a shipyard capable of servicing up to 70 vessels per year, and a commercial quay designed to accommodate vessels of up to 180 meters in

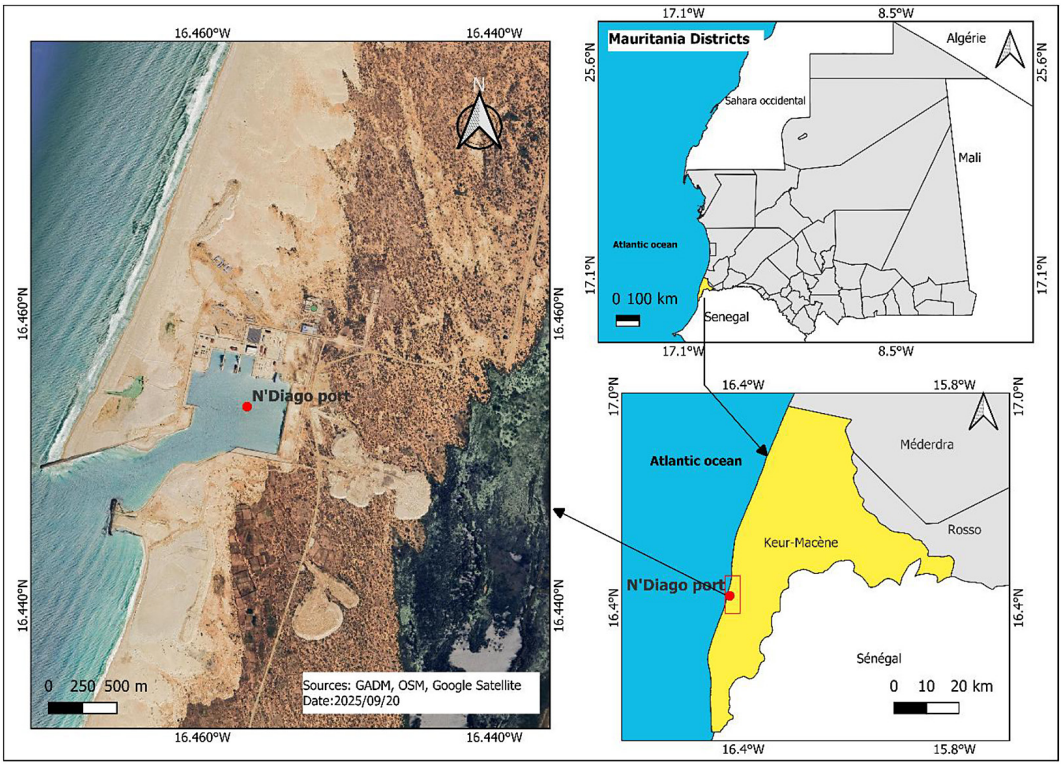

Figure 1. Geographical location of the port

length. The port was conceived to strengthen national logistical capacities, particularly to support the development of the Grand Tortue Ahmeyim gas project, while also enhancing fluvial trade connectivity toward Mali via the Senegal River.

The geographic positioning and modern facilities of the port of N'Diago confer on it a pivotal role in the economic development of southern Mauritania, as well as in the sustainable management of fisheries and energy resources. Its location at the interface of marine and fluvial domains makes it a key node for regional commerce, maritime sovereignty, and security cooperation. At the same time, the expansion of such infrastructure is likely to exert significant influence on coastal sediment dynamics and shoreline morphology, with potential implications for adjacent ecosystems and human livelihoods.

MATERIALS AND METHODS

We adopted a multi-step methodological approach in this study, summarized in the infographic presented in (Figure 2), which serves as an introductory overview before detailing the practical procedures undertaken.

Data acquisition

To analyse shoreline erosion and accretion processes in the vicinity of N'Diago Port (Mauritania), a multi-temporal and multi-sensor satellite imagery dataset was employed. The image selection relied on data acquired from Landsat 7 ETM+ (21 October 2000), Landsat 7 ETM+ (08 August 2008), Landsat 8 OLI/TIRS (12 December 2016), and Sentinel-2A MSI (05 October 2025). These sensors provide a consistent historical archive suitable for long-term shoreline monitoring, and the four acquisition dates were selected to correspond with key phases of coastal evolution relative to the construction of N'Diago Port, whose works began in 2016. All images were selected based on three criteria: (i) low cloud cover (< 20%), (ii) and acquisition during the dry season in order to minimise the influence of seasonal variability on coastal dynamics, and (iii) temporal coherence with the port construction phases.

Landsat imagery was obtained from the United States Geological Survey (USGS) Earth Explorer portal (https://earthexplorer.usgs.gov/), while the Sentinel-2A images were accessed through the Copernicus data platforms (https://browser.dataspace.copernicus.eu/) at processing level L2A (surface reflectance, atmospheric

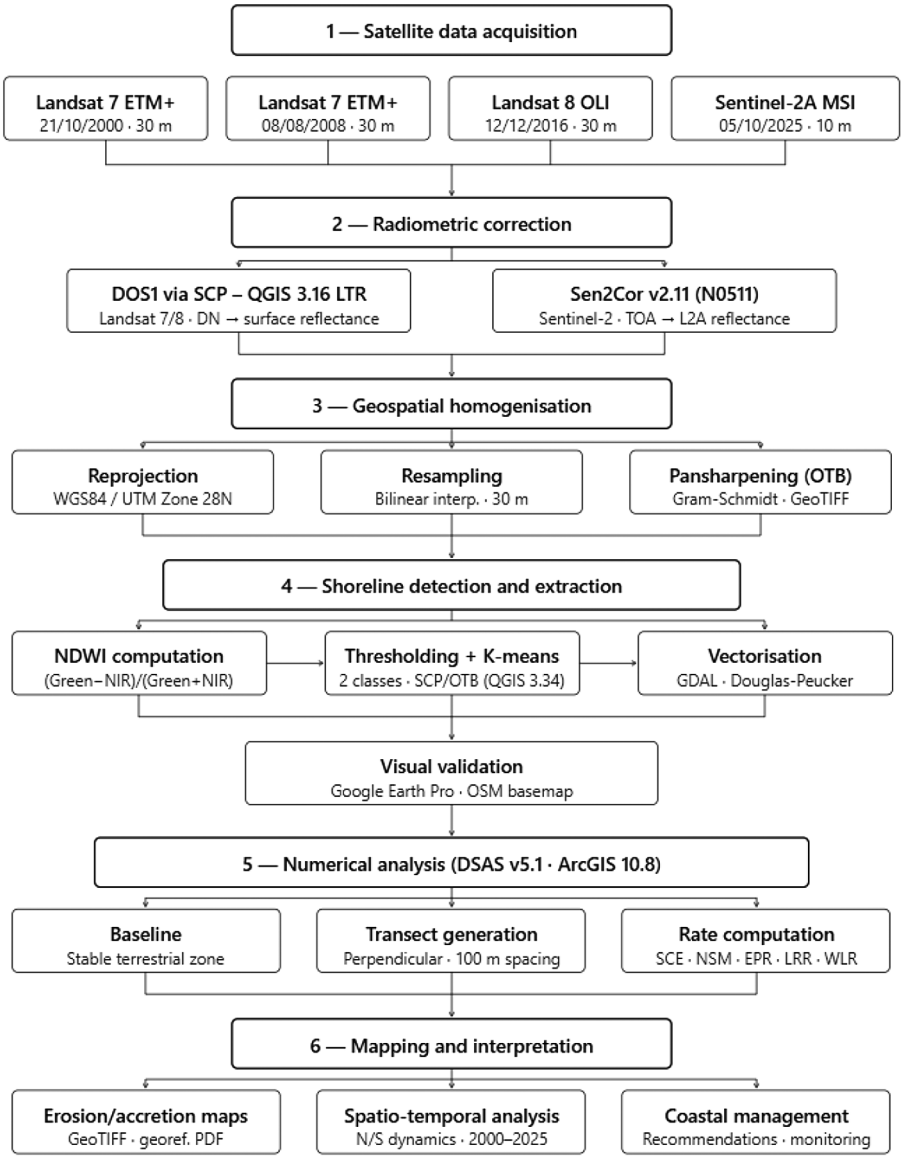

Figure 2. Methodological workflow diagram — from satellite acquisition to DSAS indicators (SCE, NSM, EPR, LRR, WLR)

correction by Sen2Cor v2.11, baseline N0511). The complete inventory of satellite scenes -including full scene identifiers, exact acquisition dates, path/row references, spatial resolution, and data sources – is provided in Table 1.

Despite originating from sensors with different spatial resolutions (30 m for Landsat, 10 m for Sentinel-2A), inter-sensor consistency was ensured through a standardised pre-processing chain. Landsat scenes (2000, 2008, 2016) underwent atmospheric correction using the DOS1 (Dark Object Subtraction) method applied via the Semi-Automatic Classification Plugin (SCP v7.10.6) within QGIS 3.16 LTR, converting raw digital numbers to surface reflectance. The Sentinel-2A scene was downloaded directly at L2A processing level, which incorporates Sen-2Cor atmospheric correction, making it directly comparable to the corrected Landsat reflectance data. All scenes were subsequently reprojected to the WGS 84/UTM Zone 28N coordinate system (EPSG: 32628) to ensure geometric consistency across the multi-source dataset.

To complement satellite-based analyses and improve shoreline delineation accuracy, high-resolution imagery from Google Earth Pro (v7.3.6) was also used for visual interpretation and cross-validation of shoreline positions for each analysed period (Warnasuriya et al., 2018). In Google Earth Pro, the historical imagery layer corresponding to each study year was selected and visually examined at a consistent

Table 1. Complete satellite image inventory with scene identifiers, exact acquisition dates, and sources

Sensor	Scene ID	Acquisition Date	Path / Row	Res. (m)	Source
Landsat 7 ETM+	LE07_L2SP_205049_20001021_20200917_02_T1	21/10/2000	205/049	30	USGS Earth Explorer
Landsat 7 ETM+	LE07_L2SP_205049_20080808_20200912_02_T1	08/08/2008	205/049	30	USGS Earth Explorer
Landsat 8 OLI	LC08_L1TP_205049_20161212_20200905_02_T1	12/12/2016	205/049	30	USGS Earth Explorer
Sentinel-2A MSI	S2A_MSIL2A_20251005T113331_N0511_R080_T28QCD	05/10/2025	Orbit 80/ T28QCD	10	Copernicus Data Space

scale (approximately 1:10,000), with the access and verification session conducted in 2025. This combined approach enhances the reliability of shoreline extraction by integrating quantitative remote sensing techniques with visual verification. Overall, the adopted data acquisition strategy provides a comprehensive and consistent basis for assessing coastal changes in the N'Diago area, supporting subsequent shoreline change analysis and coastal management applications.

Radiometric and atmospheric correction

Radiometric and atmospheric correction of Landsat imagery was performed using the Dark Object Subtraction (DOS1) method implemented through the Semi-Automatic Classification Plugin (SCP version 7.10.6) in QGIS version 3.16 LTR (Hannover), running on Windows 10/11. This approach reduces atmospheric scattering effects by subtracting the reflectance values of dark objects, identified in this study as deep water pixels and dense shadow areas, which represent the minimum DN value per band, thereby improving the temporal comparability of multi-date images. The DOS1 correction is widely applied in coastal studies due to its simplicity and robustness when detailed atmospheric data are unavailable.

The DOS1 correction was applied to all three Landsat scenes (2000, 2008, 2016) using the following parameters: dark objects were defined as the darkest pixels in each scene (deep water and dense shadows); the corrected bands included Blue, Green, Red, NIR, SWIR1, and SWIR2; digital numbers (DN) were converted to surface reflectance in the normalised range 0–1; and output rasters were produced in GeoTIFF format (Float32) projected in WGS 84 / UTM Zone 28N (EPSG: 32628).

For Sentinel-2 imagery, atmospheric correction was carried out using the Sen2Cor processor version 2.11 (Copernicus Processing Baseline N0511), which converts top-of-atmosphere (TOA) reflectance (Level-1C) into surface reflectance (Level-2A). This algorithm accounts for atmospheric effects related to aerosol optical depth, water vapour column, and Rayleigh scattering, meaning the downloaded image was already corrected and ready to use directly in the analysis. The scene was downloaded directly at L2A processing level from the Copernicus Data Space platform, with the Sen2Cor processing baseline identifier N0511 embedded in the filename (.SAFE format), confirming that atmospheric correction had already been applied. The exploited bands were B02 (Blue, 10 m), B03 (Green, 10 m), B04 (Red, 10 m), and B08 (NIR, 10 m). In practice, applying consistent correction procedures across Landsat and Sentinel-2A was a necessary step to make the reflectance values comparable before extracting shoreline positions from images acquired over a 25-year period.

Geospatial harmonization

All corrected images were reprojected into the WGS 84 / UTM Zone 28N coordinate reference system (EPSG: 32628) which is appropriate for the geographic location of the N'Diago study area. This step ensured accurate geometric alignment among all datasets. Reprojection was performed using GDAL version 3.10, integrated within QGIS. A prior verification of the spatial reference system (SRS) was conducted for each image; only those presenting an incompatibility were reprojected, preserving the native geometry of already-compliant scenes.

To address differences in spatial resolution between multispectral sensors, Specifically, a bilinear resampling method was applied via GDAL to standardise pixel size, selected over nearest-neighbour resampling for its superior spectral continuity and reduced pixellation artefacts; however, shoreline contours were extracted from each

image at its native resolution (30 m for Landsat, 10 m for Sentinel-2A) without spatial resampling, in order to preserve the geometric accuracy required for DSAS analysis. In addition, spatial enhancement techniques were used to improve geometric clarity and spectral coherence across multi-source imagery. Pansharpening using the Gram-Schmidt algorithm was applied to the Landsat 7 ETM+ scene (panchromatic band at 15 m) using the Orfeo Toolbox (OTB version 9.0.0, integrated in QGIS 3.34 Prizren) to enhance spatial detail where required. This preprocessing workflow ensured spatial consistency before any comparative or temporal analysis. All preprocessed images were exported in GeoTIFF format with complete metadata, including coordinate reference system, spatial resolution, pixel type (Float32), and acquisition date, guaranteeing data traceability and reproducibility of the analytical procedures.

Shoreline detection and extraction

Shoreline extraction was based on a three-step semi-automated approach. First, the normalized difference water index (NDWI) was computed using sensor-specific spectral bands according to Equation 1.

$$NDWI = (Green - NIR) / (Green + NIR) \quad (1)$$

The NDWI efficiently discriminates water bodies from terrestrial surfaces, with positive values (NDWI > 0) generally corresponding to water (McFeeters, 1996), and non-positive values (NDWI ≤ 0) to emerged land. The spectral bands used per sensor to compute the NDWI are detailed in Table 2. The NDWI threshold of zero (NDWI = 0) was adopted as the theoretical water–land boundary reference, consistent with the original formulation of McFeeters (1996), and was used as a baseline for cross-validation with the K-means classification results.

Second, a dynamic thresholding procedure based on image-specific local histogram analysis was applied to reclassify each NDWI raster into a binary water–land mask. This adaptive approach mitigates classification bias introduced by inter-scene variability in solar illumination geometry, atmospheric residuals, and sensor radiometric response – all of which can systematically shift the NDWI distribution and render a fixed global threshold suboptimal across a multi-sensor, multi-temporal dataset. Third, an unsupervised clustering segmentation using the K-means algorithm was implemented to generate optimal partitions into two classes, further improving the robustness of shoreline delineation. The K-means classification was applied using two tools depending on the sensor: the SCP plugin (QGIS 3.16 LTR) for Landsat 7 ETM+ (2000) and Landsat 8 OLI, and the Orfeo Toolbox (OTB 9.0.0, QGIS 3.34 Prizren) for Landsat 7 ETM+ (2008) and Sentinel-2A MSI. The parameters applied were: number of classes = 2 (water / land); maximum number of iterations = 100; convergence threshold = 0.001; random initialisation with a fixed seed to guarantee reproducibility. Results were cross-validated against the NDWI = 0 threshold as a theoretical reference.

Finally, the resulting raster boundaries were vectorized to extract shoreline contours using the GDAL 'Polygonize' tool integrated in QGIS. The water class contour was extracted and converted into a polyline representing the shoreline. Topological cleaning was applied to remove small residual features (e.g., isolated pixels or minor offshore artefacts) and to simplify shoreline geometry according to predefined thresholds: residual artefacts smaller than 500 m² were removed, and geometric simplification was performed using the Douglas-Peucker algorithm with a tolerance of 5 m. Manual digitising was additionally used to complete and refine shoreline contours where automated extraction was ambiguous. Visual validation was performed by overlaying the extracted shorelines onto OpenStreetMap (OSM) basemaps and high-resolution imagery from Google Earth Pro (v7.3.6) to assess spatial and temporal accuracy (Figure 3).

Table 2. Spectral bands used for NDWI computation per sensor

Sensor	Green band (μm)	NIR band (μm)	NDWI bands	Spatial resolution
Landsat 7 ETM+	B2 (0.52–0.60)	B4 (0.76–0.90)	B2, B4	30 m
Landsat 7 ETM+	B2 (0.52–0.60)	B4 (0.76–0.90)	B2, B4	30 m
Landsat 8 OLI	B3 (0.53–0.59)	B5 (0.85–0.88)	B3, B5	30 m
Sentinel-2A MSI	B03 (0.54–0.57)	B08 (0.78–0.90)	B03, B08	10 m

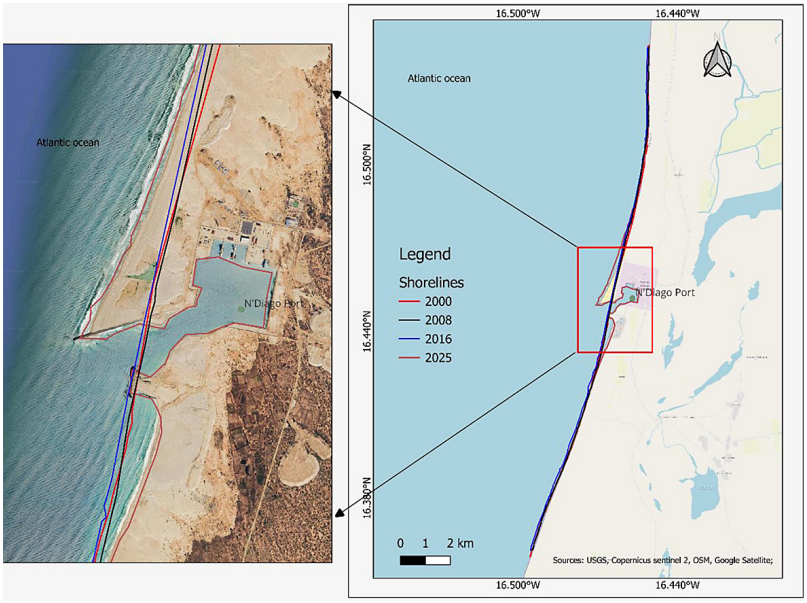

Figure 3. Shorelines extracted from Landsat and Sentinel satellite imagery (2000–2025)

Application of the digital shoreline analysis system

The digital shoreline analysis system (DSAS) is a software extension developed by the United States Geological Survey (USGS) for ArcGIS, designed to automate the temporal analysis of shoreline change based on vector shoreline datasets. In this study, DSAS version 5.1 (build 20230124.1520) was run under ArcGIS ArcMap 10.8 on Windows 10/11. DSAS generates a series of regularly spaced transects perpendicular to a user-defined baseline, allowing accurate measurement of shoreline displacement between different time periods. This standardized and reproducible approach has been widely validated and adopted for large-scale coastal change studies (Abd-Elhamid et al., 2023; Sekar et al., 2024).

Prior to running DSAS, a File Geodatabase (ESRI.gdb format) was prepared in ArcMap 10.8, integrating four shoreline vector layers corresponding to the dates 21/10/2000 (Landsat 7 ETM+), 08/08/2008 (Landsat 7 ETM+), 12/12/2016 (Landsat 8 OLI), and 05/10/2025 (Sentinel-2A MSI). Each shoreline was stored as a polyline feature class with a 'Date' attribute field formatted as required by DSAS (DD/MM/YYYY). A baseline polyline was manually digitised on the stable terrestrial side of the coast, at a sufficient distance from the shoreline to prevent any intersection with the generated transects. The geodatabase is named NDiago_DSAS.gdb and contains both the shoreline and baseline layers. The coordinate system used throughout the DSAS workflow is Mauritania 1999 / UTM Zone 28N.

Transects were generated automatically by DSAS perpendicular to the baseline, with a spacing of 100 m and a smoothing distance of 50 m. A total of 210 transects were produced, covering a 20 km coastal stretch (10 km north and 10 km south of N'Diago Port). The shoreline intersection threshold was set to 0. A default positional uncertainty of 10 m was assigned to each shoreline, and a confidence interval of 90% was applied to all statistical outputs. Bias correction was not applied.

The positional uncertainty associated with each shoreline was estimated following Fletcher et al. (2003), as the quadratic combination of three independent error components: $E_{pt} = \sqrt{(E_p^2 + E^{G2} + E^{d2})}$, where E_p is the pixel error equal to the native sensor resolution (±30 m for Landsat; ±10 m for Sentinel-2A), E^G is the georeferencing error (not applied here since all Landsat scenes are pre-georeferenced at collection level L2SP and the Sentinel-2A scene at L2A), and E^d is the digitising error estimated from spatial dispersion between manually digitised shoreline segments. Within DSAS v5.1, a uniform default positional uncertainty of ±10 m was assigned to all shoreline layers, consistent with Landsat spatial resolution, and all outputs were computed at a 90% confidence interval. The resulting mean rate uncertainties are ±0.17 m/yr (EPR) and ±4.1 m/yr (LRR/WLR), as reported in the DSAS summary file. Only transects whose estimated rate exceeds the positional uncertainty threshold are considered

statistically significant. The distribution of erosional and accretional transects per indicator, with associated statistical significance, is summarised in Table 3.

The main metrics computed by DSAS include the net shoreline movement (NSM), defined as the distance between the oldest and the most recent shoreline positions measured along a transect, expressed in meters and calculated as given in Equation 2.

$$NSM = Distance\ (oldest\ shoreline - most\ recent\ shoreline) \quad (2)$$

In addition, the shoreline change envelope (SCE) represents the maximum distance between all shoreline positions intersecting a given transect, regardless of direction, and is always positive: the SCE for the present study was calculated as given in Equation 3.

$$SCE = Distance\ (farthest\ shoreline - nearest\ shoreline) \quad (3)$$

These indicators respectively provide estimates of the net trend and the maximum amplitude of shoreline change observed over the study period (Thieler et al., 2009).

To quantify annual rates of shoreline change, DSAS computes two complementary parameters. The EPR was determined by dividing the NSM by the time interval (T) between the oldest and youngest shorelines, and was expressed as the rate of change in metres per year (see Equation 4).

$$EPR = NSM/T \quad (4)$$

The LRR (m/year) was calculated using a least squares regression line based on all the shoreline positions along each transect. This method is useful for observing shoreline evolution trends and determining linear regression rates, which correspond to long-term coastal change rates. Unlike the EPR method, the LRR method can use more than two shorelines, helping to overcome EPR's deficiency. The LRR statistical results were categorised into five groups based on the magnitude of shoreline change, following the method outlined by Zoysa et al. (2023): high accretion (> 4 m/year); low accretion (1–4 m/year); stable (−1–1 m/year); low erosion (−4−1 m/year); and high erosion (> −4 m/year). In addition, a weighted linear regression (WLR) was computed as a variant of the LRR, weighting each shoreline position by its associated positional uncertainty (default: 10 m per shoreline), thereby providing a more robust estimate where positional accuracy is uneven across dates.

Outlier handling and error assessment were integrated into the DSAS workflow as follows. Transects that did not intersect all four shoreline positions were automatically flagged and excluded from LRR and WLR calculations (resulting in 209 valid transects for these indicators, versus 210 for NSM, SCE, and EPR). The statistical reliability of each transect estimate was evaluated using the coefficient of determination (R^2), the standard error (SE), and the 90% confidence interval (CI) reported by DSAS for LRR values. Transects with $R^2 < 0.5$ or with confidence intervals exceeding the magnitude of the estimated rate were identified as statistically unreliable and interpreted with caution. No manual removal of outlier transects was performed; instead, the WLR estimator was favoured over EPR for trend interpretation, given its lower sensitivity to positional errors in individual shoreline positions.

The reliability of shoreline change estimates was further enhanced by considering statistical indicators provided by DSAS, including confidence intervals, standard error, and the coefficient of determination (R^2) associated with LRR values. The methodology required the systematic preparation of a geodatabase integrating shoreline vectors from multiple dates, the definition of a consistent baseline along the study area, and the configuration of transects adapted to the spatial resolution of the input data. A summary of the computed DSAS statistics across all 210 transects, including mean values and extreme values of SCE, NSM, EPR, LRR, and WLR, is provided in Table 4. Overall, this setup allowed us to quantify shoreline change along the N'Diago coastline in a systematic way, with results that can be verified and replicated by other researchers (Thieler et al., 2009). All output files produced during the study are available for verification and reproducibility, including the shoreline shapefiles (shoreline_2000.shp, shoreline_2008.shp, shoreline_2016.shp, shoreline_2025.shp), the DSAS geodatabase (NDiago_DSAS.gdb), the automated computation report (DSAS_Summary_TRANSECT_20250923_232416.txt), the corrected NDWI rasters in GeoTIFF format (Float32, with complete metadata), and the CSV export of SCE, NSM, EPR, LRR, and WLR values across all 210 transects.

Beyond geomorphological analysis, shoreline change rates derived from DSAS provide a robust framework for assessing the ecological impacts of coastal dynamics on marine species. Coastal infrastructures such as ports are well known to disrupt

Table 3. Erosion/accretion distribution per indicator with statistical significance

Indicator	Erosional transects (%)	Statistically significant erosion	Accretional transects (%)	Statistically significant accretion
EPR	38.1% (80/210)	34.76%	61.9% (130/210)	60.0%
LRR	42.6% (89/209)	6.7%	57.4% (120/209)	0.96%
WLR	42.6% (89/209)	6.7%	57.4% (120/209)	0.96%

Table 4. Summary of DSAS statistics across 210 transects

Indicator	No. transects	Mean value	Max. accretion	Max. erosion	Transects
SCE (m)	210	157.32 m	+614.58 m (T107)	36.45 m (T164)	T107 / T164
NSM (m)	210	+14.61 m	+267.62 m (T138)	−464.63 m (T107)	T138 / T107
EPR (m/yr)	210	+0.34 m/yr	+10.81 m/yr (T138)	−18.77 m/yr (T107)	T138 / T107
LRR (m/yr)	209	−0.35 m/yr	+8.82 m/yr (T138)	−18.12 m/yr (T107)	T138 / T107
WLR (m/yr)	209	−0.35 m/yr	+8.82 m/yr (T138)	−18.12 m/yr (T107)	T138 / T107

longshore sediment transport, generating patterns of erosion and accretion that alter beach morphology and coastal equilibrium (Nordstrom, 2014). These physical modifications are particularly critical for marine turtles, whose life cycle depends on the availability and accessibility of sandy beaches suitable for nesting (Witherington et al., 2011).

Nesting success relies on the ability of turtles to move effectively from the marine environment to appropriate beach zones, which are defined by key morphological parameters such as slope, width, and sediment characteristics. Alterations in these features can disrupt nesting behavior and influence the spatial distribution of nesting sites (Mazaris et al., 2006). In disturbed coastal environments, particularly in the vicinity of infrastructure, turtles may fail to nest or become stranded. In some cases, individuals can be overturned or trapped on modified beach profiles and are unable to return to the sea, leading to mortality (Ribeiro et al., 2025).

In this context, a total coastline length of 95,495 km encompassing the port area was mapped and subdivided into seven transect sectors (Table 5), allowing comparisons between areas located far from and near the port, as well as the number of strandings recorded over three consecutive years (2023–2025). The dataset includes 80 stranding records representing five marine turtle species (Table 6). These data were collected during stranding monitoring surveys conducted within the framework of Diawling National Park, except during periods when access to the coastline was restricted due to logistical or environmental constraints.

Species identification was carried out in the field by trained park personnel, based on a dedicated marine turtle identification guide providing detailed morphological descriptions for each species, enabling reliable distinction through carapace characteristics including shape, colouration, scale patterns, scute number and arrangement, and head morphology. Identification was primarily performed by the park conservator, the observatory manager, and the lead author of this study, all of whom have extensive field experience with marine turtles in the Diawling National Park area. For individuals presenting ambiguous or incomplete diagnostic features – particularly heavily decomposed carcasses – the record was classified as "Unidentified turtle" (n = 8; 10.0%) rather than attributed to an uncertain species. Photographic documentation was taken for each stranding event where conditions permitted, serving as a voucher record; these images are available as supplementary material.

Stranding data were organized by month and by transect and analyzed using SPSS to assess the relationship between port proximity and stranding frequency, following established approaches in coastal ecological impact studies (Defeo et al., 2009). Transects were attributed to proximity classes based on their spatial relationship to the N'Diago port infrastructure: transects T5, T6, and T7, located in the immediate vicinity of the port construction zone, were classified as "near" or "very near"; transects T1 to T4 were classified as "far". Initially, three proximity classes ("far", "near", and "very near") were defined; however, to ensure more balanced sample sizes and improve interpretability, the "near" and "very near" categories were merged. The analysis therefore considers

two groups: "far from the port" (N = 62) and "near the port" (N = 18). Descriptive statistics (mean, standard deviation, standard error, and 95% confidence intervals) were calculated to characterize data variability. All statistical analyses were performed using SPSS version 27.0.1.0 (IBM Corp., Armonk, NY, USA), with a significance level set at $\alpha = 0.05$, in accordance with standard practices in ecological data analysis. The raw SPSS data file (.sav), containing all 80 individual stranding records with their associated variables (date, transect, species, proximity class, stranding count), is available as a supplementary material.

RESULTS AND DISCUSSION

Shoreline monitoring before and after the construction of N'Diago Port (2016)

A preliminary spatial analysis of shoreline change was conducted before applying the digital shoreline analysis system (DSAS) to better understand how the coastline around the port has evolved. The comparative maps (Refer to Figure 4 and Figure 5). Clearly show that the construction of the port triggered a noticeable shift in shoreline behavior.

Before the port was built, changes along the shoreline were small and mostly fell within the range of natural variability, suggesting a coastal system that was relatively stable and close to equilibrium. After construction began, however, the shoreline underwent a significant reorganization.

A clear asymmetry appears: to the north of the port, sediments accumulated and the shoreline advanced, reflecting the trapping of sand by breakwaters and the reduction of wave energy. Meanwhile, to the south, the shoreline experienced persistent erosion, likely caused by the interruption of longshore sediment transport.

Similar behaviors have been widely documented following the construction of port infrastructures. Several studies have demonstrated that breakwaters interrupt longshore sediment transport, resulting in updrift accretion and downdrift erosion (Dean and Dalrymple, 2001). This pattern has been observed in a variety of coastal environments. For instance, shoreline modifications have been reported at Oluvil Harbor in Sri Lanka, where harbor construction altered sediment dynamics and led to distinct zones of accretion and erosion (Zoysa et al., 2023). Along the Ravenna coast in Italy, similar trends were documented, with infrastructure developments influencing historical shoreline evolution and accentuating erosion–accretion asymmetry (Sytnik et al., 2018). Comparable effects have been identified along several West African shorelines, where anthropogenic activities including port constructions significantly affect sediment distribution and shoreline change rates (Ankrah et al., 2023). Additionally, along the Rabigh coast of Saudi Arabia near King Abdullah Port, port development and associated infrastructure expansion have markedly influenced patterns of accretion and erosion (Alharbi, 2020).

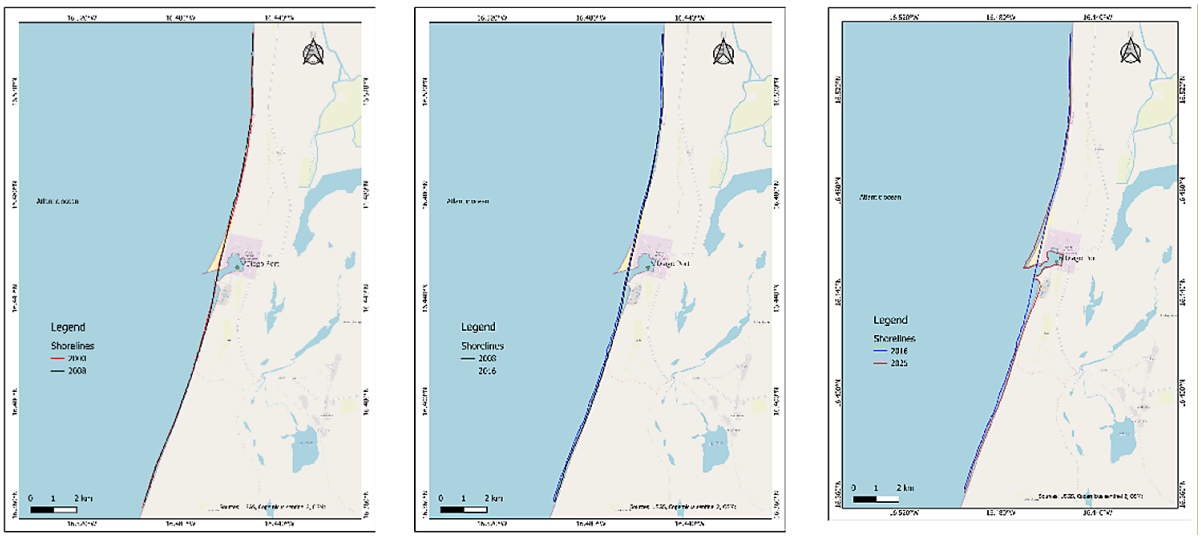

Figure 4. Shoreline evolution around N'Diago Port

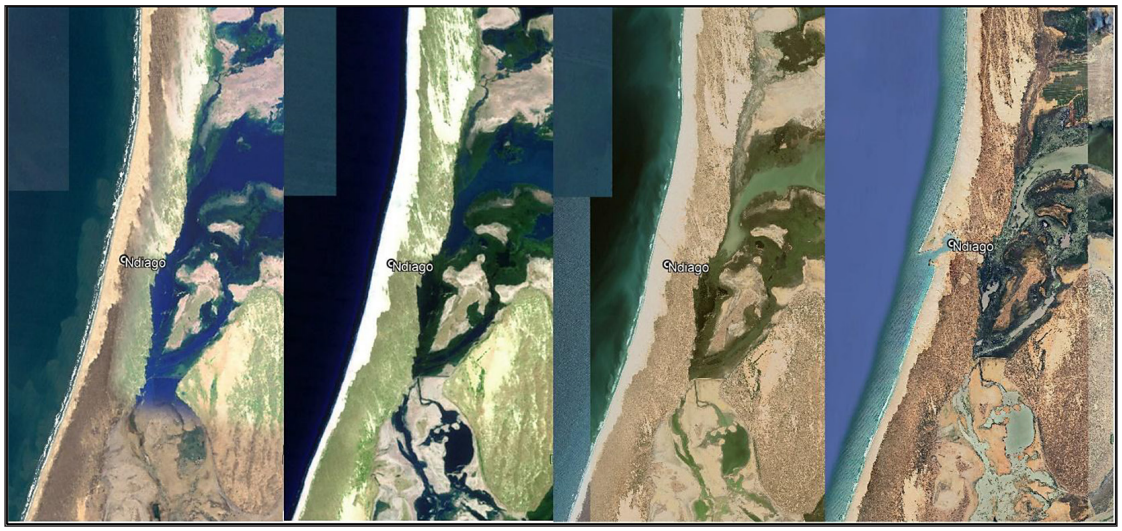

Figure 5. High-resolution satellite imagery analysis for shoreline monitoring (2000–2025)

For N'Diago Port, the year 2016 marks a turning point. From that time onward, the contrasting trends of northward accretion and southward erosion became well established. Overall, this qualitative analysis highlights that port construction has had a profound effect on coastal dynamics, reshaping sediment movement and altering the balance of the shoreline in a lasting way.

DSAS statistical analysis

The shoreline dynamics around N'Diago Port during 2000, 2008, 2016, and 2025 are illustrated in Figures 6a–6d, showing spatial contrasts and temporal trends. Figure 6a displays Net Shoreline Movement (NSM), with positive values up to +267.6 m (accretion) north of the port and negative values south, consistent over the four years. This north-south asymmetry aligns with other port-influenced coasts, such as Oluvil harbor (1991–2021, NSM –317.1 to +317.5 m), confirming the influence of port structures on sediment transport (Zoysa et al., 2023). The Shoreline Change Envelope (SCE, Figure 6b) quantifies the maximum shoreline displacement along each transect regardless of chronology, ranging from 38.45 to 614.59 m. Areas with SCE > 200 m correspond to high morphological variability near port structures, while SCE < 105 m represents relatively stable sectors. These results are comparable with engineered coasts elsewhere, where maximum SCE reached 523.8 m.

Annualized rates of shoreline change are shown via EPR and LRR. EPR (Figure 6d) varies from –18.77 to +10.81 m·yr^{-1}, highlighting strong spatial heterogeneity: severe erosion occurs south of the port, while positive rates north indicate accretion due to sediment trapping. LRR (Figure 6c), integrating all shoreline positions over the four years, ranges from –18.12 to +8.82 m·yr^{-1}, confirming these trends. The persistent erosion south and sustained accretion north demonstrate long-term sediment redistribution caused by port infrastructure (Ranasinghe, 2016).

Mapping erosion and accretion

Mapping erosion and accretion shows that 45.47 ha south of the port were eroded, whereas 111.35 ha north accreted (Figure 7 and Figure 8). This confirms artificial sediment redistribution, typical of hard infrastructure interventions (Nordstrom and Jackson, 2013). Compared with other studies, both the magnitude and asymmetry of shoreline change at N'Diago are notable, exceeding rates reported in less-engineered coasts (maximum LRR/EPR ±4–10 m·yr^{-1}).

INFLUENCE OF PORT PROXIMITY ON MARINE TURTLE STRANDINGS

To evaluate the effect of port proximity on marine turtle strandings along the N'Diago coastline, we analyzed data collected over 2023–2025 across transects classified as "near" and "far" from the port, including 80 stranding records across five marine turtle species (Table 5). A combination of ANOVA, Welch robust tests, and

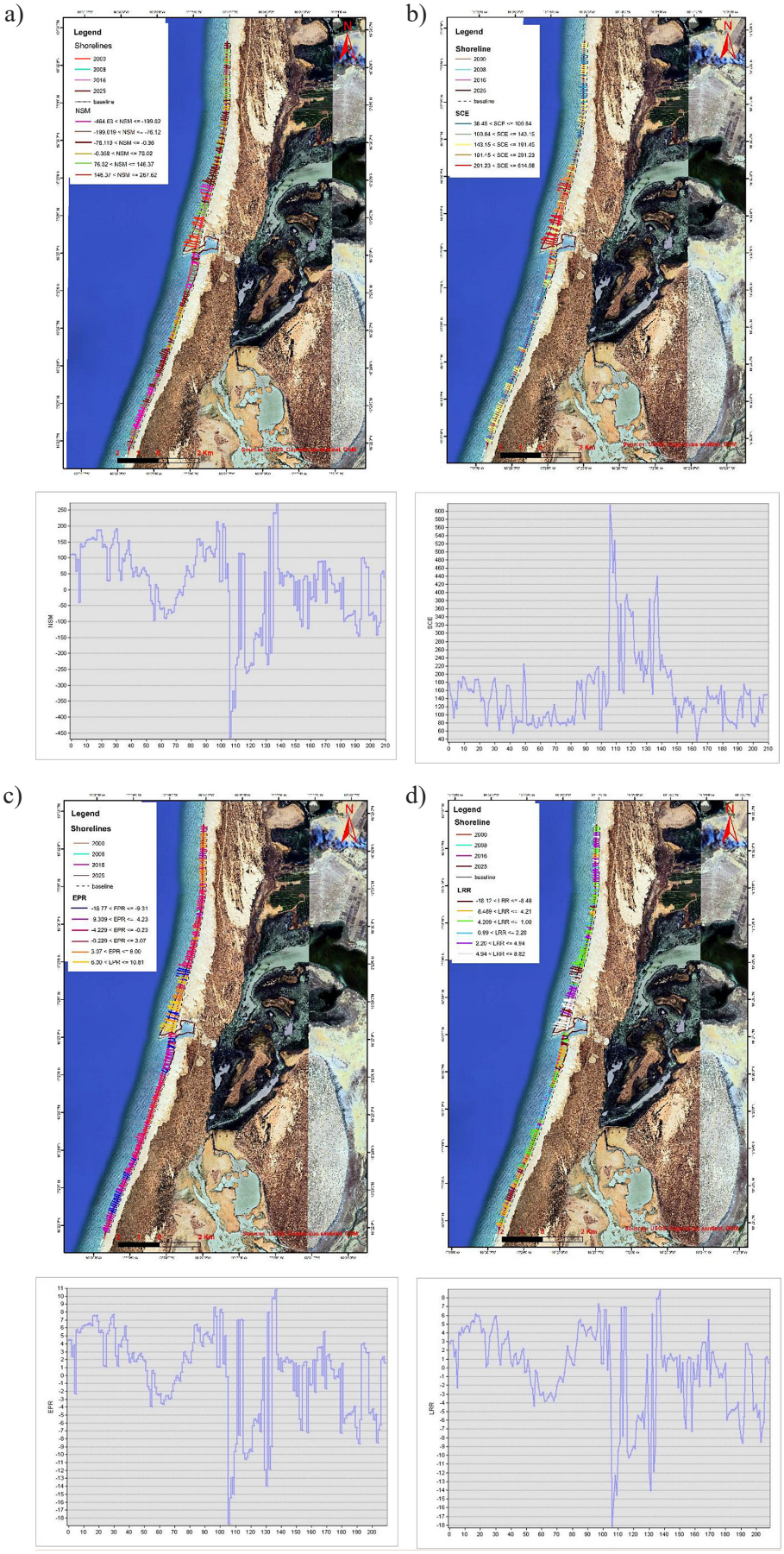

Figure 6. DSAS statistical outputs for shoreline dynamics around N'Diago Port: (a) for NSM; (b) for SCE; (c) for EPR; (d) for LRR

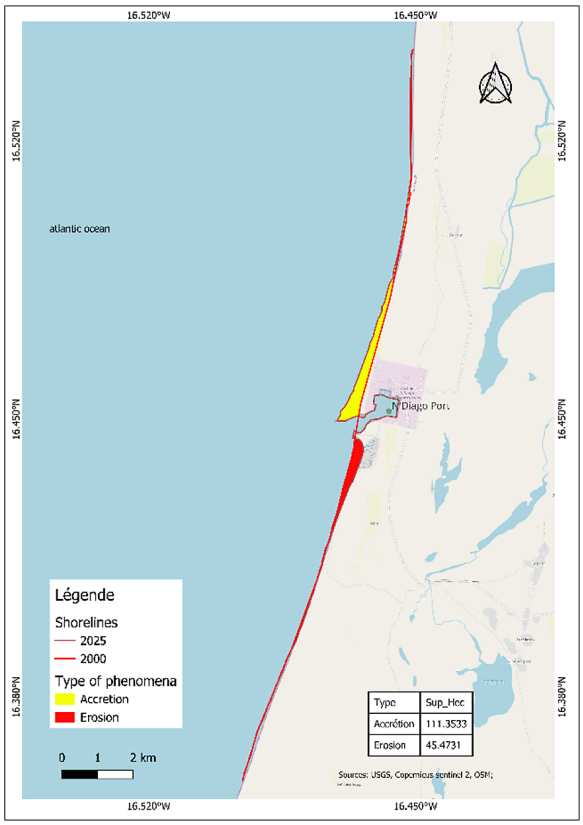

Figure 7. Erosion and accretion mapping along the N'Diago Port coastline during 2000–2025

GLM models was used to ensure robust and ecologically meaningful interpretation (Tables 7–9).

Stranding surveys were conducted as part of the coastal monitoring missions of the Diawling National Park, carried out by a dedicated team comprising the park conservator, the observatory manager, and one or two field monitoring agents. For each stranding event, a standardised observation form was completed, recording species identity, family, body measurements (length and width, measured with a measuring instrument), condition, and transect location. Each individual was marked with a coloured marker to avoid double-counting in subsequent missions. GPS coordinates were systematically recorded for each observation, and strandings were attributed to one of seven pre-defined transects (T1–T7) known to all park personnel, covering the entire study area coastline (Table 6). It is noted that survey missions were not always conducted at regular intervals, due to administrative and occasional environmental constraints; this irregularity is acknowledged as a limitation of the monitoring design.

Statistical analysis and ecological interpretation

The one-way ANOVA revealed a significant effect of port proximity on stranding frequency ($F(1, 78) = 7.290$, $p = 0.008$; Table 7), with a moderate effect size ($\eta^2 \approx 0.085$), indicating that 8.5% of the variance in strandings is explained by proximity to the port. Sites near the port showed higher mean strandings (2.72) than distant sites (1.92; Table 8). The Welch robust test confirmed this result ($F(1, 24.25) = 5.948$, $p = 0.022$; Table 9), supporting the robustness of these findings even with unequal variances and unbalanced sample sizes.

Species-level analysis shows that green turtles (*Chelonia mydas*) account for the largest proportion of strandings (40.0%), followed

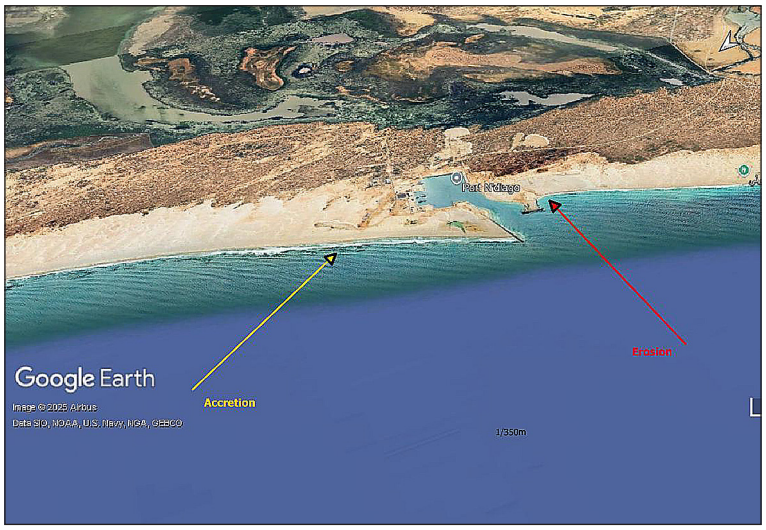

Figure 8. Eroded and accreted areas along the N'Diago Port coastline

Table 5. Species distribution of stranded marine turtles monitored during 2023–2025 (n = 80)

Espece					
Parameter		Frequency	Percent	Valid percent	Cumulative percent
Valid	Green turtle (*Chelonia mydas*)	32	40.0%	40.0%	40.0%
	Hawksbill turtle (*Eretmochelys imbricata*)	5	6.3%	6.3%	46.3%
	Leatherback turtle (*Dermochelys coriacea*)	6	7.5%	7.5%	53.8%
	Loggerhead turtle (*Caretta caretta*)	15	18.8%	18.8%	72.5%
	Olive ridley turtle (*Lepidochelys olivacea*)	14	17.5%	17.5%	90.0%
	Unidentified turtle	8	10.0%	10.0%	100.0%
	Total	80	100.0%	100.0%	

Table 6. Details of coastal transects used for stranding surveys, including GPS start and end coordinates and transect lengths

Transect	Starting point		Ending point		Length (km)
	Latitude	Longitude	Latitude	Longitude	
T1	16.98933	-16.29203	16.87414	-16.34061	13.822
T2	16.87414	-16.34061	16.78014	-16.37625	11.122
T3	16.78014	-16.37625	16.604	-16.43828	20.595
T4	16.604	-16.43828	16.47067	-16.45975	15.186
T5	16.47067	-16.45975	16.36586	-16.49258	12.186
T6	16.36586	-16.49258	16.29725	-16.51514	18.199
T7	16.29725	-16.51514	16.1675	-16.51175	4.385

Table 7. One-Way ANOVA indicating a significant effect of distance on the studied variable (p = 0.008)

Groups	Sum of squares	df	Mean square	F	Sig.
Between groups	8,992	1	8.992	7.290	.008
Within groups	96,208	78	1.233		
Total	105,200	79			

Table 8. Variation in the studied variable as a function of distance (near vs. far)

	N	Mean	Std. deviation	Std. error	95% Confidence Interval for mean		Minimum	Maximum
					Lower bound	Upper bound		
far	62	1.92	1.060	.135	1.65	2.19	1	6
near	18	2.72	1.274	.300	2.09	3.36	1	5
Total	80	2.10	1.154	.129	1.84	2.36	1	6

by loggerhead turtles (*Caretta caretta*) (18.8%) and olive ridley turtles (*Lepidochelys olivacea*) (17.5%). Leatherback (*Dermochelys coriacea*) and hawksbill (*Eretmochelys imbricata*) turtles were less frequently recorded (7.5% and 6.3%, respectively). The species-level distribution of strandings is presented in Table 4 and visually illustrated in Figure 9, which shows the frequency, percentage, and cumulative percentage of each species recorded between May 2023 and August 2025. The predominance of green turtle strandings, combined with the notable presence of loggerhead turtles near the port, is consistent with the sensitivity of both species to beach morphology alterations affecting nesting access. This result aligns with studies reporting increased strandings near coastal infrastructures (Wallace et al., 2011).

Table 9. Welch's ANOVA revealing a significant difference between group means (p = 0.022)

N	Statistics[a]	df1	df2	Sig.
Welch	5.948	1	24,248	.022
a. F asymptotically distributed				

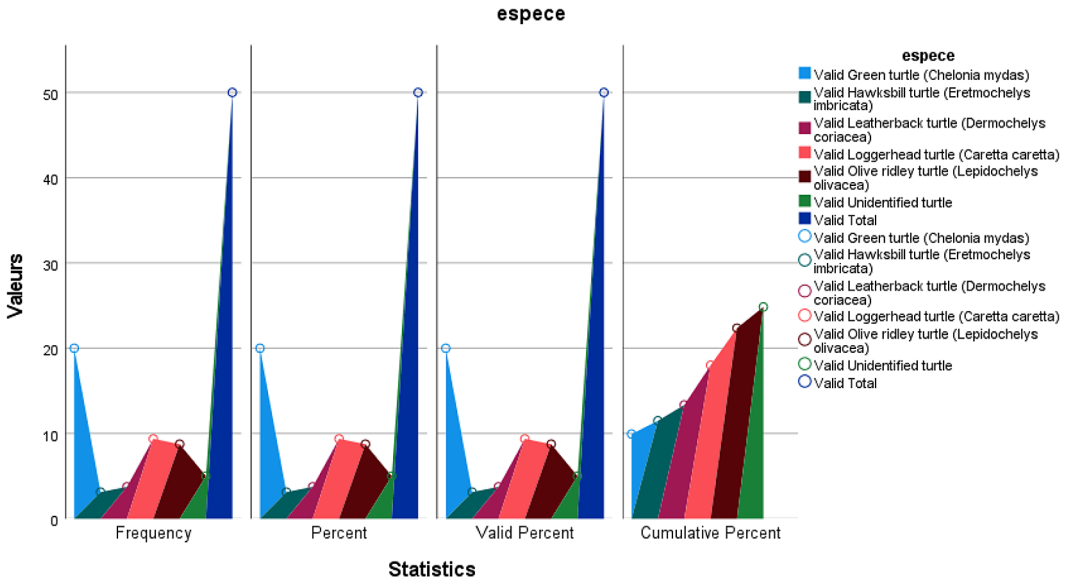

Figure 9. Species distribution of stranded sea turtles recorded between May 2023 and August 2025 along the N'Diago coastline (n = 80). The chart presents frequency, percentage, valid percentage, and cumulative percentage for each species. Green turtle (*Chelonia mydas*) was the most frequently recorded species (40%), followed by loggerhead (*Caretta caretta*, 18.8%) and olive ridley (*Lepidochelys olivacea*, 17.5%). Leatherback and hawksbill turtles represented rare stranding events (7.5% and 6.3%, respectively). Source: SPSS frequency output, Diawling National Park monitoring data (2023–2025)

GLM analysis and integrated discussion

Because stranding data are discrete counts, a generalized linear model (GLM) with Poisson distribution and log link function was applied. The GLM confirmed a significant positive association between port proximity and stranding frequency ($p < 0.05$). Importantly, *Caretta caretta* and *Chelonia mydas* showed the highest expected counts near the port, highlighting their vulnerability to anthropogenic changes in beach morphology.

Integrating these findings, the convergence of ANOVA, Welch, and GLM results demonstrates that port proximity significantly increases turtle strandings. Ecologically, port structures can obstruct nesting pathways, alter sediment transport, and modify beach slopes, which increases the likelihood of turtles being overturned or unable to return to the sea. The moderate effect size ($\eta^2 \approx 0.085$) indicates that proximity explains a substantial portion of the observed variance, but other factors such as species-specific nesting behavior, tidal cycles, and seasonal migration likely contribute to stranding patterns.

Importantly, these physical changes are closely associated with the degradation and disappearance of coastal vegetation. As demonstrated by Zoysa et al. (2023), harbor-induced shoreline changes lead to habitat loss, including vegetated zones that play a key role in sediment stabilization and nesting site suitability; they emphasize that the morphodynamic instability of areas influenced by ports accelerates the degradation of coastal ecosystems.

By referencing Tables 5,7,8, 9 and Figure 9, readers can verify species distribution, descriptive statistics, and the statistical significance of the observed differences. These results emphasize that anthropogenic coastal infrastructures have a measurable impact on marine turtle strandings and underscore the need for targeted conservation actions, such as beach restoration, monitoring, and mitigation measures near ports.

CONCLUSIONS

The construction of N'Diago Port has radically altered coastal morphodynamics, generating an asymmetric redistribution of sediments: the northern shoreline experienced substantial accretion (maximum LRR +8.82 m·yr^{-1}), while the southern shoreline underwent severe erosion (maximum LRR −18.12 m·yr^{-1}). Long-term analysis using high-resolution satellite imagery and the DSAS framework quantified shoreline transformations over 25 years, providing precise measures of NSM, SCE, EPR, and LRR for each coastal segment. Disruption of natural sediment transport coincided with an increase in marine turtle strandings near the port, confirmed by ANOVA, Welch, and GLM tests with species-specific considerations. These findings provide the first direct quantitative evidence linking engineered shoreline modifications in an arid coastal system to localized biological impacts on marine species. The results deliver unique empirical data showing how port infrastructure can drastically reshape both coastal morphology and ecosystem processes along the Mauritanian coast.

REFERENCES

1. Abd-Elhamid, H. F., Zeleňáková, M., Barańczuk, J., Gergelova, M. B., Mahdy, M. (2023). Historical trend analysis and forecasting of shoreline change at the Nile Delta using RS data and GIS with the DSAS Tool. *Remote Sensing*, *15*(7), 1737. https://doi.org/10.3390/rs15071737
2. Ankrah, J., Monteiro, A., Madureira, H. (2023). Shoreline change and coastal erosion in west africa: A systematic review of research progress and policy recommendation. *Geosciences*, *13*(2), 59. https://doi.org/10.3390/geosciences13020059
3. Davidson-Arnott, R., Bauer, B., Houser, C. (2019). Coastal geomorphology. In *Introduction to coastal processes and geomorphology* (pp. 9–28). Cambridge University Press. https://doi.org/10.1017/9781108546126.003
4. Dean, R. G., Dalrymple, R. A. (2001). *Coastal Processes with Engineering Applications*. Cambridge University Press. https://doi.org/10.1017/CBO9780511754500
5. Defeo, O., McLachlan, A., Schoeman, D. S., Schlacher, T. A., Dugan, J., Jones, A., Lastra, M., Scapini, F. (2009). Threats to sandy beach ecosystems: A review. *Estuarine, Coastal and Shelf Science*, *81*(1), 1–12. https://doi.org/10.1016/j.ecss.2008.09.022
6. Mazaris, A. D., Matsinos, Y. G., Margaritoulis, D. (2006). Nest site selection of loggerhead sea turtles: The case of the island of Zakynthos, W Greece. *Journal of Experimental Marine Biology and Ecology*, *336*(2), 157–162. https://doi.org/10.1016/j.jembe.2006.04.015
7. Mazières, A., Gillet, H., Castelle, B., Mulder, T., Guyot, C., Garlan, T., Mallet, C. (2014). High-resolution morphobathymetric analysis and evolution of Capbreton submarine canyon head (Southeast Bay of Biscay—French Atlantic Coast) over the last decade using descriptive and numerical modeling. *Marine Geology*, *351*, 1–12. https://doi.org/10.1016/j.margeo.2014.03.001
8. McFeeters, S. K. (1996). The use of the Normalized Difference Water Index (NDWI) in the delineation of open water features. *International Journal of Remote Sensing*, *17*(7), 1425–1432. https://doi.org/10.1080/01431169608948714
9. Ndour, A., Laïbi, R. A., Sadio, M., Degbe, C. G. E., Diaw, A. T., Oyédé, L. M., Anthony, E. J., Dussouillez, P., Sambou, H., Dièye, E. hadji B. (2018). Management strategies for coastal erosion problems in west Africa: Analysis, issues, and constraints drawn from the examples of Senegal and Benin. *Ocean & Coastal Management*, *156*, 92–106. https://doi.org/10.1016/j.ocecoaman.2017.09.001
10. Nordstrom, K. F., Jackson, N. L. (2013). Removing shore protection structures to facilitate migration of landforms and habitats on the bayside of a barrier spit. *Geomorphology*, *199*, 179–191. https://doi.org/10.1016/j.geomorph.2012.11.011
11. Nordstrom, K. F. (2014). Living with shore protection structures: A review. *Estuarine, Coastal and Shelf Science*, *150*, 11–23. https://doi.org/10.1016/j.ecss.2013.11.003
12. Omar A. Alharbi, O. A. A. (2020). Shoreline change analysis along the Rabigh Coast of Saudi Arabia, using multi-temporal satellite imagery. *Journal of King Abdulaziz University Marine Sciences*, *30*(2), 33–57. https://doi.org/10.4197/Mar.30-2.3
13. Ould Elmoustapha, A., Levoy, F., Monfort, O., Koutitonsky, V. G. (2007). A Numerical forecast of shoreline evolution after harbour construction in Nouakchott, Mauritania. *Journal of Coastal Research*, *236*, 1409–1417. https://doi.org/10.2112/04-0423.1
14. Ranasinghe, R. (2016). Assessing climate change impacts on open sandy coasts: A review. *Earth-Science Reviews*, *160*, 320–332. https://doi.org/10.1016/j.earscirev.2016.07.011
15. Ribeiro, L. E. S., Feitosa, Y. O., Barreto, L., Pezzuti, J. (2025). Evaluation of anthropogenic impacts on marine turtle populations in Lençóis Maranhenses National Park. *Marine Pollution*

Bulletin, *217*, 118145. https://doi.org/10.1016/j.marpolbul.2025.118145

16. Schlacher, T. A., Schoeman, D. S., Dugan, J., Lastra, M., Jones, A., Scapini, F., McLachlan, A. (2008). Sandy beach ecosystems: key features, sampling issues, management challenges and climate change impacts. *Marine Ecology*, *29*(s1), 70–90. https://doi.org/10.1111/j.1439-0485.2007.00204.x
17. Sekar, L. G., Androws, X., Annaidasan, K., Kumar, A., Kannan, R., Muthusankar, G., Balasubramani, K. (2024). Assessment of shoreline changes and associated erosion and accretion pattern in coastal watersheds of Tamil Nadu, India. *Natural Hazards Research*, *4*(2), 231–238. https://doi.org/10.1016/j.nhres.2023.09.008
18. Sytnik, O., Del Río, L., Greggio, N., Bonetti, J. (2018). Historical shoreline trend analysis and drivers of coastal change along the Ravenna coast, NE Adriatic. *Environmental Earth Sciences*, *77*(23), 779. https://doi.org/10.1007/s12665-018-7963-8
19. Thieler, E. R., Himmelstoss, E. A., Zichichi, J. L., Ergul, A. (2009). The Digital Shoreline Analysis System (DSAS) Version 4.0 - An ArcGIS extension for calculating shoreline change. *Open-File Report*.
20. Wallace, B. P., DiMatteo, A. D., Bolten, A. B., Chaloupka, M. Y., Hutchinson, B. J., Abreu-Grobois, F. A., Mortimer, J. A., Seminoff, J. A., Amorocho, D., Bjorndal, K. A., Bourjea, J., Bowen, B. W., Briseño Dueñas, R., Casale, P., Choudhury, B. C., Costa, A., Dutton, P. H., Fallabrino, A., Finkbeiner, E. M., … Mast, R. B. (2011). Global conservation priorities for marine turtles. *Plos One*, *6*(9), e24510. https://doi.org/10.1371/journal.pone.0024510
21. Fletcher, C. H., Rooney, J., Barbee, M., Lim, S. C., Richmond, B. (2003). Mapping shoreline change using digital orthophotogrammetry on Maui, Hawaii. *Journal of Coastal Research*, Special Issue 38, 106–124.
22. Warnasuriya, T. W. S., Gunaalan, K., Gunasekara, S. S. (2018). Google earth: A new resource for shoreline change estimation – case study from Jaffna Peninsula, Sri Lanka. *Marine Geodesy*, *41*(6), 546–580. https://doi.org/10.1080/01490419.2018.1509160
23. Witherington, B., Hirama, S., Mosier, A. (2011). Sea turtle responses to barriers on their nesting beach. *Journal of Experimental Marine Biology and Ecology*, *401*(1–2), 1–6. https://doi.org/10.1016/j.jembe.2011.03.012
24. Zoysa, S., Basnayake, V., Samarasinghe, J. T., Gunathilake, M. B., Kantamaneni, K., Muttil, N., Pawar, U., Rathnayake, U. (2023). Analysis of multi-temporal shoreline changes due to a harbor using remote sensing data and GIS techniques. *Sustainability*, *15*(9), 7651. https://doi.org/10.3390/su15097651